Degradation of micropollutants in secondary wastewater effluent using nonthermal plasma-based AOPs: the roles of free radicals and molecular oxidants

Changtao Chen [a, b, c], Chuanlong Ma [b], Yongyuan Yang [a], Xuetong Yang [a1*], Kristof Demeestere [c], Anton Nikiforov [b], Stijn Van Hulle [a]

[a] LIWET, Laboratory for Industrial Water and EcoTechnology, Ghent University, Campus Kortrijk, Sint-Martens - Latemlaan 2B, B-8500 Kortrijk, Belgium

[b] Research Unit Plasma Technology (RUPT), Department of Applied Physics, Ghent University, Sint - Pietersnieuwstraat 41, B4, B-9000 Ghent, Belgium

[c] Research Group Environmental Organic Chemistry and Technology (EnVOC), Department of Green Chemistry and Technology, Faculty of Bioscience Engineering, Ghent University, Coupure Links 653, B-9000, Ghent, Belgium

Abstract

Emerging micropollutants (μPs) appearing in water bodies endanger aquatic animals, plants, microorganisms and humans. The nonthermal plasma-based advanced oxidation process is a promising technology for eliminating μPs in wastewater but still

* Corresponding author

E-mail: xuetong.yang@ugent.be

needs further development in view of full-scale industrial application. A novel cascade reactor design which consists of an ozonation chamber preceding a dielectric barrier discharge (DBD) plasma reactor with a falling water film on an activated carbon textile (Zorflex®) was used to remove a selection of µPs from secondary municipal wastewater effluent. Compare to previous plasma reactor, molecular oxidants degraded micropollutants again in an ozonation chamber in this study, and the utilization of different reactive oxygen species (ROS) was improved. A gas flow rate of 0.4 standard liter per minute (SLM), a water flow rate of 100 mL min^{-1}, and a discharge power of 25 W are identified as the optimal plasma reactor parameters, and the µP degradation efficiency and electrical energy per order value (EE/O) are 84-98% and 2.4-5.3 kW/m^3, respectively. The presence of ROS during plasma treatment was determined in view of the µPs removal mechanisms. The degradation of diuron (DIU), bisphenol A (BPA) and 2-n-octyl-4-isothiazolin-3-one (OIT) was mainly performed in ozonation chamber, while the degradation of atrazine (ATZ), alachlor (ALA) and primidone (PRD) occurred in entire cascade system. The ROS not only degrade the µPs, but also remove nitrite (90.5%), nitrate (69.6%), ammonium (39.6%) and bulk organics (11.4%). This study provides insights and optimal settings for an energy-efficient removal of µPs from secondary effluent using both free radicals and molecular oxidants generated by the plasma in view of full-scale application.

Keywords

Advanced oxidation processes, Micropollutants, Nonthermal plasma, Wastewater treatment, Reactive oxygen species

1 Introduction

In recent years, the occurrence of emerging organic micropollutants (μPs) in water/wastewater has drawn much attentions. μPs include pesticides, herbicides, pharmaceuticals, plasticizers, and may result, when discharged along with wastewater effluent, in significant toxicity and environmental hazards (Lotfi et al. 2022). μPs can accumulate in the environment for a long time, which makes human exposed to potential health risks (Alsbaiee et al. 2016, Carpenter and Helbling 2018).

The conventional activated sludge process plays an irreplaceable role in wastewater treatment. However, it is difficult to remove μPs with such activated sludge processes in traditional wastewater treatment plants (WWTPs) (Helbling et al. 2012). Hence, the (secondary) effluent of WWTPs is regarded as the main pathway through which μPs enter the aquatic environment, and the concentration of μPs in wastewater ranges from ng/L to mg/L (See Table S1, in Supplementary Information, SI).

Advanced Oxidation Processes (AOPs) are effective methods to remove μPs from secondary effluent by in-situ production of hydroxyl radicals (·OH) and other highly reactive oxygen species (ROS) (Singh et al. 2020). ROS are divided into free radicals

(i.e. ·OH, superoxide radicals ($O_2^{\bullet-}$), singlet oxygen ($^1O_2$)) and molecular oxidants (i.e. hydrogen peroxide (H_2O_2), ozone (O_3)) (Singh et al. 2019a). Molecular oxidants have a longer lifetime than free radicals, as shown in Table S2, SI. The role of free radicals on μPs removal has already been emphasized previously, but the function of molecular oxidants seems to be overlooked. In fact, some μPs with specific structures (e.g. double bonds, aromatic rings) are easily oxidized by O_3. Zhang et al. found that H_2O_2 played an indispensable role in carbamazepine removal by directly reacting with the target μPs or promote the generation of ·OH (Zhang et al. 2022).

Nonthermal plasma-based AOPs are a novel type of AOPs which generate a high-density plasma through a high-voltage discharge. Both free radicals and molecular oxidants can be generated in a typical plasma system by a series of physical and chemical reactions (Shang et al. 2022). These ROS, including ·OH, $O_2^{\bullet-}$, $^1O_2$, H_2O_2, and O_3, can degrade μPs. Nonthermal plasma-based AOPs have the unique advantages of strong oxidation ability, short treatment time, no external chemical addition, and limited secondary pollution. However, previous studies on μPs removal by plasma mainly take advantage of the free radicals in the plasma zone which results in the loss of molecular oxidants along with the exhaust (Singh et al. 2019b). Efficient use of O_3 and other molecular oxidants during plasma treatment is key to enhance the plasma treatment performance. The removal behavior of μPs in secondary wastewater effluent by plasma-based AOPs has rarely been studied. Previous studies typically focus on the use of plasma treatment to remove μPs from synthetic wastewater(Vanraes et al. 2017,

Vanraes et al. 2015, Wardenier et al. 2019a, Wardenier et al. 2019b, Wardenier et al. 2019c). However, the complexity of the real wastewater composition is an important obstacle for the full-scale application of plasma treatment, since it reduces the effectiveness of AOPs for wastewater remediation. A variety of inorganics, organics and microorganisms may compete for oxidants and impede the removal of μPs. Moreover, current studies mostly work with plasma treatment systems operated in batch mode. However, the output of secondary municipal wastewater effluent is huge, and batch mode is unpractical for full-scale applications.

In order to tackle the challenges above, a novel cascade reactor configuration was developed to remove μPs from secondary municipal wastewater effluent operating in continuous mode. It consists of a dielectric barrier discharge (DBD) plasma reactor with a falling water film on an activated carbon textile (Zorflex®), that is connected in series with a preceding ozonation chamber. The μPs are firstly ozonated in the ozonation chamber, and then degraded by ROS in the plasma chamber. Compared to previous studies mainly focusing on free radicals' production in nonthermal plasma-based AOP, here the utilization of different ROS was achieved in this novel cascade reactor configuration. The reactor was operated in a single-pass mode, assuring continuous operation in view of μPs removal from real wastewater. The effects of operational parameters and wastewater composition on the μPs removal performance were comprehensively evaluated. Furthermore, ROS generation in different water matrices was compared. The economic/energy cost of the entire cascade system for μPs removal

in secondary effluent was also evaluated.

2 Materials and Methods

2.1 Secondary wastewater and reagents

The secondary effluent was collected from a WWTP in Belgium, and stored at 4 ℃ before treatment. It does not exceed 2 days before treatment. Properties of the secondary effluent used in this work are given in Table 1.

Table 1 Here

The concentration of naturally occurring micropollutant varied a lot due to wastewater source, season, weather and so on. If naturally occurring micropollutants were used, degradation efficiency of micropollutants after plasma treatment will be different due the changes of the initial concentration of micropollutants. Spiking target micropollutants with a fixed concentration in the secondary effluent is therefore a better choice. Furthermore, the applied concentration of micropollutants enables the detection after treatment. Thus, atrazine (ATZ), alachlor (ALA), diuron (DIU), primidone (PRD), 1,7-α-ethinylestradiol (EE2), bisphenol A (BPA), and 2-n-octyl-4-isothiazolin-3-one (OIT) were selected as model μPs in this study. The physical-chemical properties of these μPs are given in Table S3 and S4 in SI. The selected μPs were dissolved in deionized water, resulting in a stock solution with individual μPs at a concentration of 5.0 mg/L. According to Table S1, the μPs concentration in real secondary wastewater

effluent of WWTPs ranges between 0.01 μg/L and 250 μg/L. Therefore, the stock solution was diluted to the desired concentration (200 μg/L) using secondary effluent. The stock solution was diluted with ultrapure water to obtain synthetic wastewater with a μPs concentration of 200 μg/L.

2.2 Setup and experimental procedures

A schematic representation of the DBD plasma reactor is shown in Figure. 1. Detailed information about the reactor can be found in our previous work (Vanraes et al. 2017, Vanraes et al. 2015, Wardenier et al. 2019a, Wardenier et al. 2019b, Wardenier et al. 2019c). In short, wastewater flows through the ozonation and plasma chambers in a sequence. A stainless-steel tube was placed inside the quartz glass tube. The stainless-steel tube was used as the grounded inner electrode, which was covered by 2 layers of activated carbon textile. The wastewater was pumped up from the ozonation chamber through the stainless-steel pipe, and then flowed down the activated carbon textile. Plasma was generated using oxygen gas on the activated carbon textile by applying a pulsed high voltage to an outer mesh electrode covering a quartz glass tube. Next, produced O_3 and residual O_2 gas mixtures were bubbled into the ozonation chamber.

Figure 1. Here

A pulse generator model TGP110 Thulby Thandar instrument was used to trigger the AC high voltage power supply working at 50 kHz, and modulated the sinusoidal voltage waveform using a square wave function. The modulated waveform was defined

by a plasma 'on' time of 5 ms (T_{on}) and a plasma 'off' time of 45 ms (T_{off}). The duty cycle was defined as following:

$$DC = \frac{T_{on}}{T_{on}+T_{off}} = 10\% \quad (1.)$$

A Tektronix® TD 1002 digital oscilloscope was used to monitor the voltage and current waveforms using a Tektronix® P6015 A HV probe and an IonPhysics® current probe, respectively. The total input power (P) used to generate the plasma was calculated by multiplying the duty cycle with the instantaneous power delivered to the reactor (P_0),

$$P = P_0 * DC \quad (2.)$$

The ozonation chamber was filled with 600 mL wastewater. The wastewater was pumped from the ozonation chamber to the plasma chamber at a designed liquid flow (from 60 to 100 mL/min). A falling water film was formed on the activated carbon textile (Zorflex®). The gas entered the bottom of the plasma chamber at a designed gas flow (from 0.4 to 1 standard liter per minute, SLM). Finally, the wastewater after treatment was sampled and analyzed. The details of the analytical methods are given in Section 2.5. The reactor performance was evaluated in terms of removal efficiency and energy consumption. The removal efficiency of the µPs (R) was defined as follows:

$$R = \frac{c_0 - c_t}{c_t} * 100\% \quad (3.)$$

where c_0 is the initial concentration of the µPs (200 µg L^{-1}) and c_t (µg L^{-1}) is the final concentration of the µPs. Energy consumption was characterized by the electrical energy per order (EE/O, kWh/m³) figure-of-merit (Yang et al. 2021), as shown

in eq. (4):

$$EE/O = \frac{P}{F * \log(\frac{c_o}{c_t})} \quad (4.)$$

where P (kW) is the total input power used to generate the plasma in the reactor, which was calculated by eq. (2), and F ($m^3\ h^{-1}$) is the liquid flow. All experiments were performed thrice, and the average value was adopted.

For the treatment based on ozonation alone, only the ozonation chamber is used. The ozonation chamber was filled with 600 mL wastewater. The wastewater was only treated in the ozonation chamber, and it flowed out from ozonation chamber directly, and did not flow into plasma chamber. The gas entered the bottom of the plasma chamber at a gas flow of 1 SLM, and then entered the ozonation chamber via a diffuser.

For the treatment based on plasma alone, only the plasma chamber is used. The plasma chamber was fed with 600 mL. The gas entered the bottom of the plasma chamber at a gas flow of 1 SLM. Wastewater did not enter the ozonation chamber and it passed through the plasma chamber only once.

2.3 Design of response surface methodology modeling

The response surface methodology (RSM) based on the Box–Behnken design (BBD) method was used to optimize the operational parameters of the reactor (Chys et al. 2015). Three independent variables included gas flow rate, liquid flow rate, and discharge power, as shown in Table 2. The discharge power is related to the generation of ROS, and both the gas and liquid flow rates might affect the mass transfer of ROS.

As reported in a previous study, ATZ, as a typical recalcitrant contaminant in wastewater, is difficult to remove in the plasma reactor (Wardenier et al. 2019c). Its removal efficiency is lower than that of other μPs, such as ALA, DIU, dichlorvos, pentachlorophenol, carbamazepine, EE2, BPA (Wardenier et al. 2019c). Thus, the removal efficiency and energy consumption for ATZ removal were selected as response factors, and the effects of those operational parameters on the response factor are studied. The corresponding RSM model can be found in Eq.5,

$$y_i=a+bX_1+cX_2+dX_3+eX_1X_2+fX_1X_3+gX_2X_3+hX_1^2+iX_2^2+jX_3^2 \quad (5)$$

in which y_i represents the response factor for the removal efficiency of ATZ (y_R, %) as well as for the energy consumption of ATZ removal ($y_{EE/O}$, kWh/m³). X_1, X_2 and X_3 refer to gas flow rate (SLM), liquid flow rate (mL min^{-1}) and discharge power (W), respectively. Multiple regression was used to estimate the coefficients a to j, based on the experimental conditions and the measured results (namely y_R or $y_{EE/O}$).

Table 2. Here

2.4 Free radical quenching experiment

p-benzoquinone, 1,4-diazabicyclo octane, and tert-butanol were used as scavenger to quench the $\cdot O_2^-$, $^1O_2$, and ·OH, respectively (Lou et al. 2022). Each scavenger was added into synthetic wastewater, and the concentration of each scavenger was set at 20 mmol L^{-1}. Synthetic wastewater containing scavenger was treated through the entire cascade system at the optimal parameters. The detailed experiment procedure was

shown in Section 2.2.

2.5 Analytical methods

The concentration of μPs was determined by an Agilent gas chromatography–mass spectrometry system (GC-MS, 6890 series GC system, 5973 MS) adapted from previous research (Yang et al. 2022), and a detailed procedure is outlined in Text S1, SI. H_2O_2 concentrations were measured by the titaniumoxysulphate method (Pandiyaraj et al. 2021). The indigo method was used to measure the concentration of dissolved ozone in liquid (Bader and Hoigné 1981). $\int [O_3]dt$ and $\int [H_2O_2]dt$ were the exposures of O_3 and H_2O_2, and were obtained from the time-integrated the concentration of O_3 and H_2O_2 over the treatment time (Guo et al. 2021). The details are given in Text S2, SI. ·OH exposures were indirectly measured by the terephthalic acid method (See Text S3, SI) (Liu et al. 2021).

The concentrations of nitrite (NO_2^-), nitrate (NO_3^-), ammonium (NH_4^+), and Chemical Oxygen Demand (COD) were determined according to standard methods using the commercial Hach test kits coupling with an ultraviolet-visible spectrophotometer (DR2800, Hach, Belgium). The pH and conductivity of the wastewater were measured using portable pH and conductivity meter, respectively (HQ30d, HACH, US). The three-dimensional excitation-emission matrix (3D-EEM) fluorescence spectra of samples were determined by a fluorescence spectrophotometer (RF-5301 PC, Shimadzu, Japan). The details of 3D-EEM measurements and data

processing are given in Text S4, SI. The ultraviolet-visible spectroscopy (UV-vis) spectra of samples were recorded by an ultraviolet-visible spectrophotometer (DR2800, Hach, Belgium) in the wavelength range between 200 nm and 800 nm.

Synergistic effect between plasma and ozonation was evaluated by the synergistic index, which was calculated by the Eq. (5),

$$\text{Synergistic index} = \frac{k_{\mu Ps,\ plasma+ozonation}}{k_{\mu Ps,\ plasma} + k_{\mu Ps,\ ozonation}} \quad (5)$$

where $k_{\mu Ps,\ plasma+ozonation}$, $k_{\mu Ps,\ plasma}$ and $k_{\mu Ps,\ ozonation}$ (min^{-1}) were the apparent pseudo-first order reaction constants of μPs degradation for plasma + ozonation, plasma alone, ozonation alone.

3 Results and Discussion

3.1 RSM approach and statistical analysis

3.1.1 Establishment of model equations and data fitting

In the first step, the efficiency and energy consumption of ATZ removal in secondary wastewater effluent were selected as response factors to build an appropriate RSM approach. The operational parameters, experimental and predicted results of removal efficiency and EE/O are shown in Table S5. The experimental results show that the ATZ removal efficiency and energy consumption ranged between 90 – 98% and 4.0 – 7.0 kWh/m³, respectively. A good agreement between the experimental and the predicted results was achieved for both the removal efficiency (y_R, R^2 = 0.98, the

number of datapoints included in the regression: n = 17) and energy consumption ($y_{EE/O}$, $R^2 = 0.99$, n = 17). The model equations were established as follow:

$$y_R=88+1.1X_1+28X_2+4.5X_3+0.02X_1X_2+0.3X_1X_3+0.3X_2X_3+0.2X_1^2+1.1X_2^2+1.6X_3^2 \quad (6)$$

$$y_{EE/O}=12+0.1X_1+4.3X_2+5.2X_3+0.02X_1X_2+0.006X_1X_3+0.0006X_2X_3+0.02X_1^2+0.6X_2^2+1.2X_3^2 \quad (7)$$

The model for ATZ removal efficiency and energy consumption, the coefficients corresponding to the gas flow (X_1), liquid flow (X_2) and discharge power (X_3) are statistically significant ($p < 0.05$, See Table S6, SI). The absolute values of the coefficients represent how significantly the different operational parameters affect the ATZ removal efficiency and energy consumption. The significance sequence of each factor is: discharge power (C) > liquid flow rate (B) > gas flow rate (A).

3.1.2 Influence of operational parameters on efficiency and energy consumption of atrazine removal

Surface plots of RSM in terms of the removal efficiency and energy consumption are shown for ATZ at different operational parameters in Figure. S1 and S2. As Run 5 and 8 indicated (Table S5), the removal efficiency increased by 6% but the energy consumption increased by 28% when the discharge power increased from 25 W to 45 W. The increase of input power achieved by an increase of the applied voltage can increase the electric field in the reactor, and facilitate the dissociation, ionization and excitation of the feed gas (Kim et al. 2013), thereby generating more ROS (Sun et al. 1997). As such, a higher μPs removal efficiency can be obtained at higher input power

conditions, but the energy consumption increases as well. From an economical point of view, a lower input power is beneficial for the commercial application of the plasma reactor. According to the requirements of the Swiss water protection act, the removal efficiency of μPs was recommended not less than 80% (Bourgin et al. 2018). When the discharge power was 25 W, the removal efficiency of μPs was higher than 85%, and the energy consumption was merely 4.0 kWh/m^3, indicating the high removal efficiency and energy-efficient properties of the plasma reactor. As such, in this context, the optimal discharge power can be determined as 25 W.

When the liquid flow rate increased from 60 to 100 mL min^{-1}, the removal efficiency and energy consumption reduced by 5% and 33%, respectively (See Run 10 and 12, in Table S5). Indeed, the removal efficiency of μPs decreased with the increase of liquid flow rate, because the residence time of the ROS in the ozonation and plasma chamber is shortened at faster liquid flow rates. In other words, a higher liquid flow rate shortens the reaction time of ROS and μPs. The energy consumption reduces as the liquid flow increases, which is in agreement with our previous studies (Wardenier et al. 2019c). For energy consumption, the optimum liquid flow rate was found to be 100 mL min^{-1}.

As indicated in Figure. S1, when the gas flow rate increased from 0.4 to 0.8 SLM, the removal efficiency was reduced slightly. This phenomenon can be caused by the complex interactions between the gas flow and the generation of plasma/ROS. An excessive gas flow rate reduces the contact time between gas molecules and also affects

277 the transfer of ROS from gas to liquid phase, which is not conducive to the degradation
278 of μPs (Aggelopoulos et al. 2020). In addition, an excessively large gas flow rate can
279 greatly shorten the residence time of the ROS in the ozonation chamber, which reduces
280 the utilization rate of ROS. A higher gas flow rate also causes a sharp increase in the
281 consumption of feed gas, and increases the operational costs. Therefore, for removal
282 efficiency and energy consumption, 0.4 SLM was defined as the optimum gas flow rate.

283 3.2 Removal of micropollutants at optimal conditions

284 3.2.1 Micropollutants

285 Both secondary effluent and synthetic wastewater containing seven μPs (DIU, OIT,
286 ATZ, ALA, BPA, EE2, and PRD) were treated at the optimized operational conditions.
287 As shown in Figure. 2 (A, B), the removal efficiencies of the seven μPs were all over
288 85%, and they were ranked as BPA > EE2 > OIT > DIU > ATZ > ALA > PRD. The
289 energy consumption in case of secondary effluent is between 2.4 kW/m³ and 5.3 kW/m³,
290 whereas the energy consumption for synthetic wastewater is between 2.3 kW/m³ and
291 4.8 kW/m³. It should be noted that there is no significant difference for energy
292 consumption in between synthetic wastewater and real wastewater in this study. It
293 indicates that this reactor can overcome the negative influences brought by a complex
294 water matrix composition well. Compared to nonthermal plasma-based AOPs in
295 previous literatures in Table 3, the plasma reactor used in this study performs very well

296 in terms of removal efficiency and energy consumption. This is attributed to the
297 improved utilization of ROS in this reactor. Compare to previous plasma reactor,
298 molecular oxidants degraded μPs again in an ozonation chamber in this novel cascade
299 reactor configuration. Thus, higher removal efficiency and lower energy consumption
300 were achieved.

301 **Figure 2**. Here

302 **Table 3**. Here

303 **3.2.2 Contribution of plasma and ozonation**

304 Secondary effluent containing micropollutants was treated by plasma chamber and
305 ozonation chamber respectively. The contribution of plasma and ozonation chamber on
306 the degradation of μPs was evaluated. The degradation efficiencies of μPs after
307 treatment with plasma & ozonation were about 30%-50% higher than that of treated by
308 plasma alone or ozonation alone. The presence of ozonation chamber promoted the
309 degradation efficiency of μPs and reduced the energy consumption. Because the
310 utilization of ROS in entire cascade system is enhanced. The degradation kinetics of
311 BPA treated by plasma + ozonation, plasma alone and ozonation alone were shown in
312 Figure S5. The synergistic index of BPA degradation between plasma and ozonation
313 was 3.43. As such, a strong synergistic effect on the degradation of μPs was noticed. In
314 addition, the degradation efficiencies of EE2, BPA, OIT treated by plasma alone were
315 about 15-25% lower than that treated by ozonation alone. It indicates that the
316 degradation of EE2, BPA, OIT depends on the oxidation of O_3. Liu et al. found that

317 those μPs were easily degraded by O_3, as their double bonds and aromatic rings were
318 destroyed (Liu et al. 2020). The degradation efficiencies of DIU, ATZ and ALA were
319 not significantly different after treatment with ozonation alone and plasma alone.
320 Previous works shown that the reaction constants between O_3 and DIU, ATZ, ALA were
321 small, and the degradation of DIU, ATZ and ALA was closely related to the act of free
322 radicals (Meephon et al. 2019, Plaza et al. 2021). The degradation of DIU, ATZ and
323 ALA in ozonation chamber was attributed to the free radicals generated by the
324 decomposition of molecular oxidants.

325 **Figure 3**. Here

326 **3.2.3 Inorganic nitrogen**

327 The changes of some common water quality parameters of real wastewater
328 including concentrations of pH, conductivity, nitrite, nitrate and ammonium were
329 measured as well. The pH value of the secondary effluent varied between 6.99 and 7.10
330 after treatment, with little change. The conductivity was reduced from 629 μS/cm to
331 605 μS/cm after treatment. This may be related to the decrease of nitrite, nitrate and
332 ammonium concentration. The removal efficiencies of nitrite, nitrate and ammonium at
333 the optimized operational conditions were 90.5±4.2%, 69.6±5.5% and 40.0±7.7%,
334 respectively. Nitrite and nitrate react with ·OH, H_2O_2, and O_3, as shown in Eq.(R1) -
335 (R4) (Bradu et al. 2020, Lukes et al. 2014, Zhou et al. 2020). Due to the generation of
336 solvated electrons, nitrite and nitrate may be reduced, and then N_2 can be produced.

Ammonium can react with ·OH and O_3, and then N_2, nitrite and nitrate can be generated, as shown in Eq.(R5) - (R8) (Wu et al. 2020). Normally, tertiary inorganic nitrogen removal from the secondary effluent can be accomplished by biological methods, adsorption or ion exchange (Amini et al. 2018, Liu et al. 2019a, Yi et al. 2020). Nonthermal plasma-based AOPs can degrade μPs in wastewater while removing inorganic nitrogen at the same time, without additional chemicals or technology. The results obtained in this work open a window to remove inorganic nitrogen from secondary effluent.

$$2NO_2^- + H^+ + H_2O_2 \rightarrow ONOOH + H_2O \quad (R1)$$

$$NO_2^- + O_3 \rightarrow NO_3^- + O_2 \quad (R2)$$

$$NO_2^- + \cdot OH \rightarrow \cdot NO_2 + OH^- \quad (R3)$$

$$NO_3^- + \cdot OH \rightarrow \cdot NO_3 + OH^- \quad (R4)$$

$$NH_4^+ + 3 \cdot OH \rightarrow 0.5N_2 + H^+ + 3H_2O \quad (R5)$$

$$NH_4^+ + 3 \cdot OH \rightarrow 0.5NO_2 + 3H^+ + 2H_2O \quad (R6)$$

$$NH_4^+ + 3 \cdot OH \rightarrow 0.5NO_3 + 2H^+ + 1.5H_2O \quad (R7)$$

$$NH_4^+ + O_3 \rightarrow 0.5N_2 + H^+ + 1.5H_2O \quad (R8)$$

3.2.3 Bulk organic matter

The secondary effluent contains a large amount of high molecular weight organic pollutants. These complex mixtures usually consist of hydrophilic and hydrophobic

356 substances, such as proteins, humic acids and fulvic acids. They can be degraded to
357 lower molecular weight compounds by ROS. The total dissolved solids (TDS) were
358 reduced from 570 mg/L to 550 mg/L. This can be attributed to the removal of organic
359 matters. The removal efficiency of COD at the optimized operational conditions was
360 11.4±3.6%. Kim et al. found that improving the carbon mineralization efficiency is
361 much more difficult than enhancing target μPs removal efficiency during nonthermal
362 plasma-based AOPs (Kim et al. 2013). In case mineralization would be required, the
363 addition of catalysts or combining plasma with other AOPs should be investigated.
364 The changes of high molecular weight organic pollutants after treatment with the
365 plasma reactor were analyzed using 3D-EEM and UV-vis spectra (Figure. 4). Three
366 peaks (A, B, C peak) in the 3D-EEM spectra were observed in the original real
367 wastewater, representing proteins, fulvic acids and humic acids, respectively (Chen et
368 al. 2021). All peaks in the real wastewater after plasma treatment disappeared. It
369 indicates that proteins, humic and fulvic acids were removed.
370 Ultraviolet absorbance is an important indicator for organic pollutants in
371 secondary effluent. Various compounds containing aromatic hydrocarbons and
372 conjugated systems of double bonds or hydroxyl groups are the main organic pollutants
373 in secondary effluent (accounting for 40% to 60% of dissolved organic carbon)
374 (Anumol et al. 2015). These organic pollutants have strong absorption peaks at the
375 ultraviolet wavelength of 254 nm (Anumol et al. 2015). The absorbance at 254 nm
376 (UV_{254}) of secondary effluent after plasma treatment was reduced by 48%. The

reduction of absorbance indicates that the organic pollutants were degraded.

Figure 4. Here

3.3 The removal mechanisms of micropollutants

3.3.1 Generation of reactive oxidative species

The generation of ROS (e.g. H_2O_2, O_3, and ·OH) was investigated in different types of water, over a period of 10 min. The exposures of all investigated ROS were higher in ultrapure water than in synthetic wastewater and real wastewater (Figure. 5) indicating that ROS are consumed due to the presence of μPs and the co-existent inorganic and organic matter in the secondary effluent. Therefore, compared with other water matrices, the exposures of ROS in secondary effluent were the lowest. For each water matrix, the exposures of ·OH generated by the plasma were the lowest, followed by O_3 and H_2O_2. Taking the ROS in ultrapure water as an example, the maximum exposures of ·OH, O_3 and H_2O_2 were 2.93×10^{-11}, 0.07, and 0.28 (M s), respectively. In general, H_2O_2 does not directly participate in the degradation of μPs, but indirectly reacts with μPs by generating free radicals (Aggelopoulos et al. 2020). As shown in Eq.(R9) and (R10), an important source of ·OH is the reaction between O_3 and H_2O_2. Thus, the contents of H_2O_2 and O_3 in all water matrices reduced with time, whereas the contents of ·OH increased with time. The reaction rates of various micropollutants with ·OH and O_3 are shown in Table S4. The reaction rates and concentration of ·OH are larger than those of O_3. Therefore, ·OH will play a more important role in

397 removing μPs.

398 $$H_2O_2+O_3 \rightarrow \cdot OH+HO_2\cdot+O_2 \quad (R9)$$

399 $$H_2O_2 + 2\ O_3 \rightarrow 3\ O_2 + 2\cdot OH \quad (R10)$$

400 **Figure 5**. Here

401 **3.3.2 Role of various radicals**

402 In nonthermal plasma-based AOPs, various strong oxidizing radicals can be
403 produced in large quantities, and the production of these radicals (·OH, $O_2^{\bullet-}$, $^1O_2$) will
404 have an impact on the removal of μPs. In order to study the role of various radicals in
405 the removal of μPs during plasma treatment, radical trapping experiments were
406 conducted by adding scavengers to synthetic wastewater (Figure. 6). The removal of
407 μPs was inhibited because of the addition of scavengers (e.g., p-benzoquinone, 1,4-
408 diazabicyclo octane, and tert-butanol), but the effects of them on each μP were different.
409 More than 95% of EE2 was removed even in the presence of scavengers. The absence
410 of free radicals did not have a large impact on EE2 removal. When $O_2^{\bullet-}$ and $^1O_2$ were
411 quenched, the removal efficiency of BPA was reduced by 40-55%. As such, it can be
412 seen that $O_2^{\bullet-}$ and $^1O_2$ are important oxidizing radicals rather than ·OH for the removal
413 of BPA, which is in line with previous work (Yang et al. 2018). The removal efficiency
414 of OIT decreased from 98.7±0.4% to 71.3±2.6% in the absence of $O_2^{\bullet-}$. The removal
415 efficiency of OIT did not reduce much without $^1O_2$ and ·OH. The removal efficiency
416 of DIU dropped by 30%-40% after scavenging $O_2^{\bullet-}$ and ·OH. $O_2^{\bullet-}$ and ·OH are

417 responsible to degrade the DIU, as also demonstrated by Meephon et al (Meephon et al.
418 2019). Three kinds of free radicals have effect on the removal of ATZ, among which
419 ·OH has the most significant effect. Plaza et al. found that ·OH played a vital role to
420 degrade ATZ and its alkylic oxidation (Plaza et al. 2021). The removal efficiency of
421 ALA and PRD reduced by about 35%-40% in the absence of $O_2^{\bullet-}$ and ·OH, while the
422 effect of $^1O_2$ on their removal was not significant. The oxidation pathway of ALA in a
423 plasma reactor was studied by Bolobajev et al (Bolobajev et al. 2021). They confirmed
424 that the removal of ALA starts with the attack of ·OH, and includes dehalogenation,
425 electrophilic attack of the aromatic ring, ether bond cleavage, and cyclisation. Liu et al.
426 assessed the contribution of ROS in the photochemical catalysis of PRD, and found that
427 ·OH play the most critical role in PRD removal (Liu et al. 2019b). This is because active
428 sites in the PRD molecular structure that are easily fractured by ·OH are mainly
429 aromatic rings and methylene groups between two nitrogen atoms. The investigation
430 reveals that the role of ROS in the removal of μPs in plasma are type-specific, but the
431 co-existence of various efficient ROS in controlled plasmas can provide a possible fit-
432 for-all solution for μPs removal from wastewater.

433 **Figure 6**. Here

434 **3.3.3 Effect of co-existent inorganic and organic matter**

435 Nitrate (NO_3^-), ammonium (NH_4^+), nitrite (NO_2^-), carbonate (CO_3^-) and humic acids
436 (HA) are typically present in secondary effluent. These inorganic and organic

components were spiked in the synthetic wastewater, and their effects on the μPs removal efficiency was investigated. The five co-existent components had no obvious reducing effect on the removal of BPA and EE2, even at a quite high concentration. The removal efficiency of BPA and EE2 was more than 92% (Figure. 7). HA and NO_2^- had a more remarkable reducing effect on the degradation of DIU, OIT, ATZ and ALA than other ions. HA is a ubiquitous natural organic matter found in most groundwater, surface water and wastewater. HA competes with μPs for reaction with ROS and therefore interferes with the removal of μPs. So μPs decomposition is significantly reduced at constant energy input. H_2O_2, O_3, ·OH and other ROS that played a crucial role in the removal of μPs were rapidly consumed by NO_2^- (Bradu et al. 2020, Lukes et al. 2014, Zhou et al. 2020). Fortunately, NO_2^- concentration in the secondary effluent is generally less than 1 mg/L (Table 1). PRD was difficult to remove in the plasma reactor, and the five co-existent components had a significant inhibitory effect on its removal efficiency as it dropped by about 20-30%. NO_3^- and CO_3^- are scavengers of radicals, and can react with ·OH (Fan et al. 2021). Fan et al. found that NH_4^+ reacts with ·OH and $^1O_2$, through which N_2, NO_3^- and NO_2^- may be generated (Fan et al. 2021). Finally, the removal efficiency was thus reduced and extra energy input may be required due to the complex matrix compositions.

Figure 7. Here

4 Conclusions

In this study, a DBD plasma reactor with a falling water film on an activated carbon textile (Zorflex®) preceded by an ozonation chamber connected in series was used to treat secondary effluent containing seven μPs (ATZ, ALA, PRD, DIU, OIT and BPA). Compare with previous plasma reactor, the two chambers in this cascade system enabled full-scale utilization of both free radicals and molecular oxidants produced by highly reactive plasmas. The degradation efficiencies of μPs after treatment with entire cascade system were about 30%-50% higher than that of treated by plasma alone or ozonation alone. At the optimized operational conditions, the energy consumption of real wastewater treatment was between 2.4 kW/m³ and 5.3 kW/m³, while that of synthetic wastewater was between 2.3 kW/m³ and 4.8 kW/m³.

Furthermore, this study also shows that plasma can not only degrade μPs but also nitrite, nitrate, ammonium, and COD in secondary effluent. The exposures of ·OH generated by the plasma were the lowest, followed by O_3 and H_2O_2. The removal of DIU, OIT, and BPA were mainly affected by $O_2^{\bullet-}$, and the removal of ATZ, ALA, and, PRD were closely related to the ·OH. The results of this study provide useful information for developing effective technologies to treat real wastewater, which is helpful in the control and remediation of μPs.

Acknowledgement

Changtao Chen (Grant No. 202106240063), Chuanlong Ma, Yongyuan Yang and Xuetong Yang are financially supported by the China Scholarship Council (CSC) by a CSC Ph.D. grant.

Reference

Aggelopoulos, C.A., Meropoulis, S., Hatzisymeon, M., Lada, Z.G. and Rassias, G. (2020) Degradation of antibiotic enrofloxacin in water by gas-liquid nsp-DBD plasma: Parametric analysis, effect of H2O2 and CaO2 additives and exploration of degradation mechanisms. Chemical Engineering Journal 398.

Alsbaiee, A., Smith, B.J., Xiao, L., Ling, Y., Helbling, D.E. and Dichtel, W.R. (2016) Rapid removal of organic micropollutants from water by a porous β-cyclodextrin polymer. Nature 529(7585), 190-194.

Amini, N., Papineau, I., Storck, V., Bérubé, P.R., Mohseni, M. and Barbeau, B. (2018) Long-term performance of biological ion exchange for the removal of natural organic matter and ammonia from surface waters. Water Research 146, 1-9.

Anumol, T., Sgroi, M., Park, M., Roccaro, P. and Snyder, S.A. (2015) Predicting trace organic compound breakthrough in granular activated carbon using fluorescence and UV absorbance as surrogates. Water Research 76, 76-87.

Bader, H. and Hoigné, J. (1981) Determination of ozone in water by the indigo method. Water Research 15(4), 449-456.

Bolobajev, J., Gornov, D., Kornev, I. and Preis, S. (2021) Degradation of aqueous alachlor in pulsed corona discharge. Journal of Electrostatics 109, 103543.

Bourgin, M., Beck, B., Boehler, M., Borowska, E., Fleiner, J., Salhi, E., Teichler, R., von Gunten, U., Siegrist, H. and McArdell, C.S. (2018) Evaluation of a full-scale wastewater treatment plant upgraded with ozonation and biological post-treatments: Abatement of micropollutants, formation of transformation products and oxidation by-products. Water Research 129, 486-498.

Bradu, C., Kutasi, K., Magureanu, M., Puač, N. and Živković, S. (2020) Reactive nitrogen species in plasma-activated water: generation, chemistry and application in agriculture. Journal of Physics D: Applied Physics 53(22), 223001.

Carpenter, C.M.G. and Helbling, D.E. (2018) Widespread Micropollutant Monitoring in the Hudson River Estuary Reveals Spatiotemporal Micropollutant Clusters and Their Sources. Environmental Science & Technology 52(11), 6187-6196.

Chen, C., Zhang, T., Lv, L., Chen, Y., Tang, W. and Tang, S. (2021) Destroying the structure of extracellular polymeric substance to improve the dewatering performance of waste activated sludge by ionic liquid. Water Research 199, 117161.

Chys, M., Declerck, W., Audenaert, W.T.M. and Van Hulle, S.W.H. (2015) UV/H2O2, O3 and (photo-) Fenton as treatment prior to granular activated carbon filtration of biologically stabilized landfill leachate. Journal of Chemical Technology & Biotechnology 90(3), 525-533.

Fan, J., Wu, H., Liu, R., Meng, L., Fang, Z., Liu, F. and Xu, Y. (2021) Non-thermal plasma combined with zeolites to remove ammonia nitrogen from wastewater. Journal

of Hazardous Materials 401, 123627.

Guo, Y., Zhan, J., Yu, G. and Wang, Y. (2021) Evaluation of the concentration and contribution of superoxide radical for micropollutant abatement during ozonation. Water Research 194, 116927.

Helbling, D.E., Johnson, D.R., Honti, M. and Fenner, K. (2012) Micropollutant Biotransformation Kinetics Associate with WWTP Process Parameters and Microbial Community Characteristics. Environmental Science & Technology 46(19), 10579-10588.

Kim, K.-S., Yang, C.-S. and Mok, Y.S. (2013) Degradation of veterinary antibiotics by dielectric barrier discharge plasma. Chemical Engineering Journal 219, 19-27.

Liu, Y., Ngo, H.H., Guo, W., Peng, L., Wang, D. and Ni, B. (2019a) The roles of free ammonia (FA) in biological wastewater treatment processes: A review. Environment International 123, 10-19.

Liu, Y., Wang, Q., Wang, C., Zhang, A., Huang, K., Liu, J., Miruka, A.C., Han, Q. and Guo, Y. (2021) Degradation of dichloroacetic acid in a novel corona discharge reactor integrated with microbubbles generation. Separation and Purification Technology 274, 119019.

Liu, Y., Yan, S., Lian, L., Ma, J., Zhou, H. and Song, W. (2019b) Assessing the contribution of hydroxylation species in the photochemical transformation of primidone (pharmaceutical). Science of The Total Environment 696, 133826.

Liu, Z., Yang, Y., Shao, C., Ji, Z., Wang, Q., Wang, S., Guo, Y., Demeestere, K. and Hulle, S.V. (2020) Ozonation of trace organic compounds in different municipal and industrial wastewaters: Kinetic-based prediction of removal efficiency and ozone dose requirements. Chemical Engineering Journal 387, 123405.

Lotfi, S., Fischer, K., Schulze, A. and Schäfer, A.I. (2022) Photocatalytic degradation of steroid hormone micropollutants by TiO2-coated polyethersulfone membranes in a continuous flow-through process. Nature Nanotechnology 17(4), 417-423.

Lou, J., Lu, G., Wei, Y., Zhang, Y., An, J., Jia, M. and Li, M. (2022) Enhanced degradation of residual potassium ethyl xanthate in mineral separation wastewater by dielectric barrier discharge plasma and peroxymonosulfate. Separation and Purification Technology 282, 119955.

Lukes, P., Dolezalova, E., Sisrova, I. and Clupek, M. (2014) Aqueous-phase chemistry and bactericidal effects from an air discharge plasma in contact with water: evidence for the formation of peroxynitrite through a pseudo-second-order post-discharge reaction of H2O2and HNO2. Plasma Sources Science and Technology 23(1), 015019.

Meephon, S., Rungrotmongkol, T., Puttamat, S., Praserthdam, S. and Pavarajarn, V. (2019) Heterogeneous photocatalytic degradation of diuron on zinc oxide: Influence of surface-dependent adsorption on kinetics, degradation pathway, and toxicity of

intermediates. Journal of Environmental Sciences 84, 97-111.

Pandiyaraj, K.N., Vasu, D., Ghobeira, R., Tabaei, P.S.E., De Geyter, N., Morent, R., Pichumani, M., Padmanabhanan, P.V.A. and Deshmukh, R.R. (2021) Dye wastewater degradation by the synergetic effect of an atmospheric pressure plasma treatment and the photocatalytic activity of plasma-functionalized Cu–TiO2 nanoparticles. Journal of Hazardous Materials 405, 124264.

Plaza, J., Arencibia, A. and López-Muñoz, M.J. (2021) Evaluation of nZVI for the degradation of atrazine in heterogeneous Fenton-like systems at circumneutral pH. Journal of Environmental Chemical Engineering 9(6), 106641.

Shang, K., Morent, R., Wang, N., Wang, Y., Peng, B., Jiang, N., Lu, N. and Li, J. (2022) Degradation of sulfamethoxazole (SMX) by water falling film DBD Plasma/Persulfate: Reactive species identification and their role in SMX degradation. Chemical Engineering Journal 431, 133916.

Singh, R.K., Fernando, S., Baygi, S.F., Multari, N., Thagard, S.M. and Holsen, T.M. (2019a) Breakdown Products from Perfluorinated Alkyl Substances (PFAS) Degradation in a Plasma-Based Water Treatment Process. Environmental Science & Technology 53(5), 2731-2738.

Singh, R.K., Multari, N., Nau-Hix, C., Anderson, R.H., Richardson, S.D., Holsen, T.M. and Mededovic Thagard, S. (2019b) Rapid Removal of Poly- and Perfluorinated Compounds from Investigation-Derived Waste (IDW) in a Pilot-Scale Plasma Reactor. Environmental Science & Technology 53(19), 11375-11382.

Singh, R.K., Multari, N., Nau-Hix, C., Woodard, S., Nickelsen, M., Mededovic Thagard, S. and Holsen, T.M. (2020) Removal of Poly- and Per-Fluorinated Compounds from Ion Exchange Regenerant Still Bottom Samples in a Plasma Reactor. Environmental Science & Technology 54(21), 13973-13980.

Sun, B., Sato, M. and Sid Clements, J. (1997) Optical study of active species produced by a pulsed streamer corona discharge in water. Journal of Electrostatics 39(3), 189-202.

Vanraes, P., Ghodbane, H., Davister, D., Wardenier, N., Nikiforov, A., Verheust, Y.P., Van Hulle, S.W.H., Hamdaoui, O., Vandamme, J., Van Durme, J., Surmont, P., Lynen, F. and Leys, C. (2017) Removal of several pesticides in a falling water film DBD reactor with activated carbon textile: Energy efficiency. Water Res 116, 1-12.

Vanraes, P., Willems, G., Nikiforov, A., Surmont, P., Lynen, F., Vandamme, J., Van Durme, J., Verheust, Y.P., Van Hulle, S.W., Dumoulin, A. and Leys, C. (2015) Removal of atrazine in water by combination of activated carbon and dielectric barrier discharge. J Hazard Mater 299, 647-655.

Wardenier, N., Gorbanev, Y., Van Moer, I., Nikiforov, A., Van Hulle, S.W.H., Surmont, P., Lynen, F., Leys, C., Bogaerts, A. and Vanraes, P. (2019a) Removal of alachlor in water by non-thermal plasma: Reactive species and pathways in batch and continuous process. Water Res 161, 549-559.

Wardenier, N., Liu, Z., Nikiforov, A., Van Hulle, S.W.H. and Leys, C. (2019b)

Micropollutant elimination by O3, UV and plasma-based AOPs: An evaluation of treatment and energy costs. Chemosphere 234, 715-724.

Wardenier, N., Vanraes, P., Nikiforov, A., Van Hulle, S.W.H. and Leys, C. (2019c) Removal of micropollutants from water in a continuous-flow electrical discharge reactor. J Hazard Mater 362, 238-245.

Wu, H., Fan, J., Chen, W. and Yang, C. (2020) Dielectric barrier discharge-coupled Fe-based zeolite to remove ammonia nitrogen and phenol pollutants from water. Separation and Purification Technology 243, 116344.

Yang, S., Wu, P., Liu, J., Chen, M., Ahmed, Z. and Zhu, N. (2018) Efficient removal of bisphenol A by superoxide radical and singlet oxygen generated from peroxymonosulfate activated with Fe0-montmorillonite. Chemical Engineering Journal 350, 484-495.

Yang, X., De Buyck, P.-J., Zhang, R., Manhaeghe, D., Wang, H., Chen, L., Zhao, Y., Demeestere, K. and Van Hulle, S.W.H. (2022) Enhanced removal of refractory humic- and fulvic-like organics from biotreated landfill leachate by ozonation in packed bubble columns. Science of The Total Environment 807, 150762.

Yang, X., Liu, Z., Manhaeghe, D., Yang, Y., Hogie, J., Demeestere, K. and Van Hulle, S.W.H. (2021) Intensified ozonation in packed bubble columns for water treatment: Focus on mass transfer and humic acids removal. Chemosphere 283, 131217.

Yi, C., Qin, W. and Wen, X. (2020) Renovated filter filled with poly-3-hydroxybutyrateco-hydroxyvalerate and granular activated carbon for simultaneous removal of nitrate and PPCPs from the secondary effluent. Science of The Total Environment 749, 141494.

Zhang, L., Chen, J., Zhang, Y., Xu, Y., Zheng, T. and Zhou, X. (2022) Highly efficient activation of peracetic acid by nano-CuO for carbamazepine degradation in wastewater: The significant role of H2O2 and evidence of acetylperoxy radical contribution. Water Research 216, 118322.

Zhou, R., Zhou, R., Wang, P., Xian, Y., Mai-Prochnow, A., Lu, X., Cullen, P.J., Ostrikov, K. and Bazaka, K. (2020) Plasma-activated water: generation, origin of reactive species and biological applications. Journal of Physics D: Applied Physics 53(30), 303001.

Figure Captions

Figure 1. Schematics of the setup with plasma chamber (right) and ozonation chamber (left) (Vanraes et al. 2017, Vanraes et al. 2015, Wardenier et al. 2019a, Wardenier et al. 2019b, Wardenier et al. 2019c).

Figure 2. The efficiency and energy consumption of μPs degradation at the optimized operational parameters. (A). Removal efficiencies. (B). Energy consumption.

Figure 3. The efficiency and energy consumption of μPs degradation after treatment with plasma & ozonation, plasma alone, ozonation alone. (A). Removal efficiencies. (B). Energy consumption.

Figure 4. 3D-EEM and UV-vis spectra of real wastewater. (A). 3D-EEM spectra: original real wastewater. (B). 3D-EEM spectra: real wastewater after treatment. (C). UV-vis spectra.

Figure 5. Exposures of ROS in the different water matrix. (A). Exposure of ·OH. (B). Exposure of O_3. (C). Exposure of H_2O_2.

Figure 6. Effects of various radicals on the removal efficiency of μPs.

Figure 7. Effect of different co-existent inorganic and organic matter on the efficiency and energy consumption of μPs removal. (A). Removal efficiencies. (B). Energy consumption. (The concentration of each co-existent component is 20 mg/L.)

18 **Figure 1**

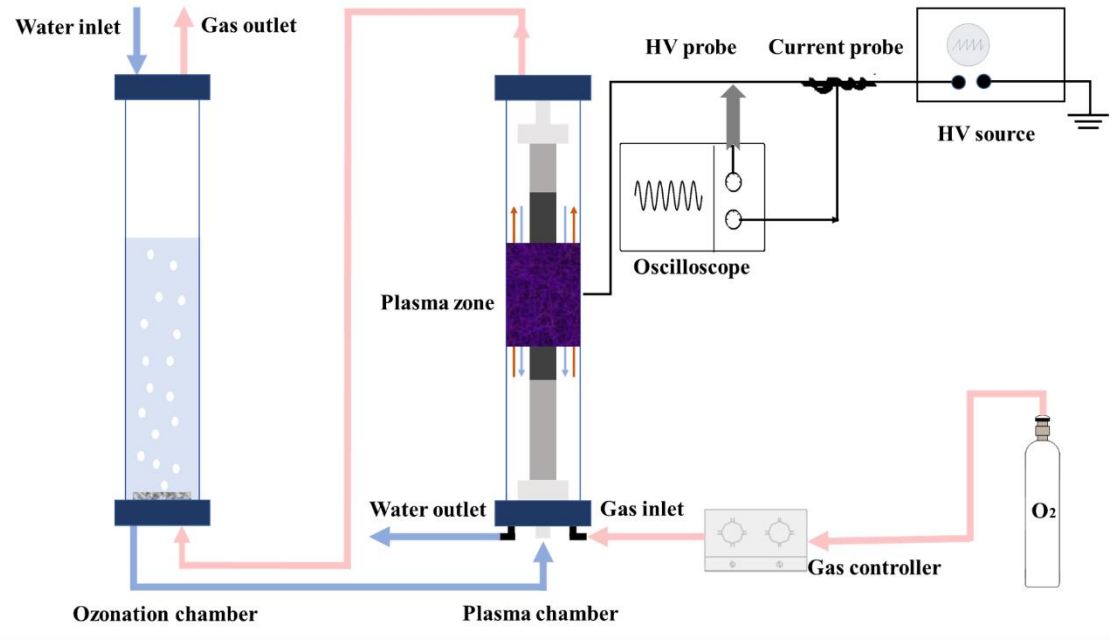

19

Figure 2

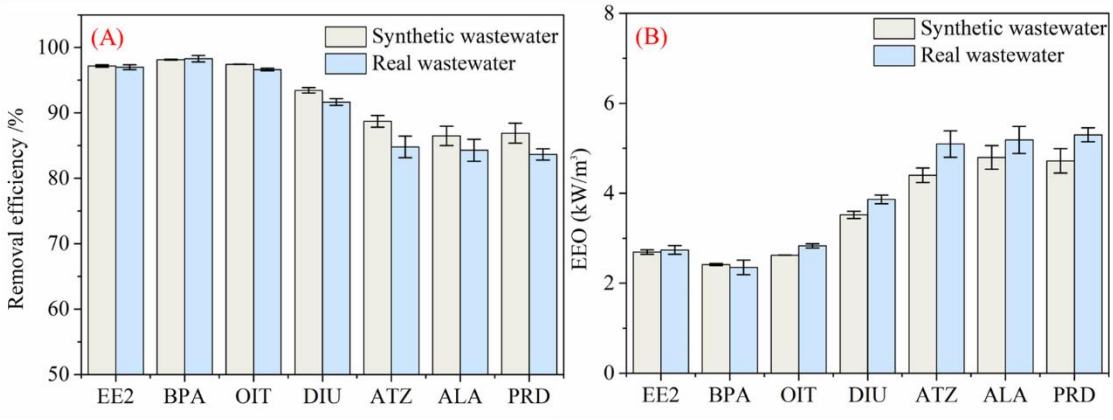
(A)
Synthetic wastewater
Real wastewater
Removal efficiency /%
100
90
80
70
60
50
EE2
BPA
OIT
DIU
ATZ
ALA
PRD
(B)
Synthetic wastewater
Real wastewater
EEO (kW/m³)
8
6
4
2
0
EE2
BPA
OIT
DIU
ATZ
ALA
PRD

22 **Figure 3**

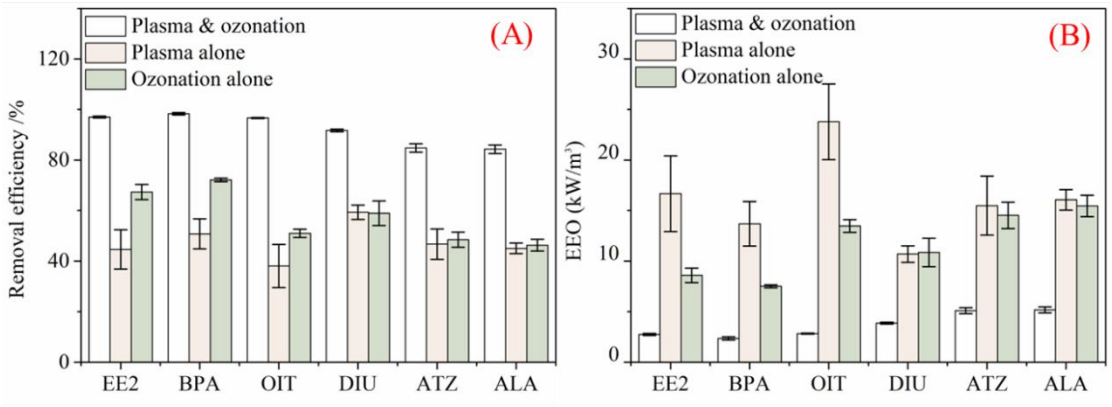

23

24 **Figure 4**

25 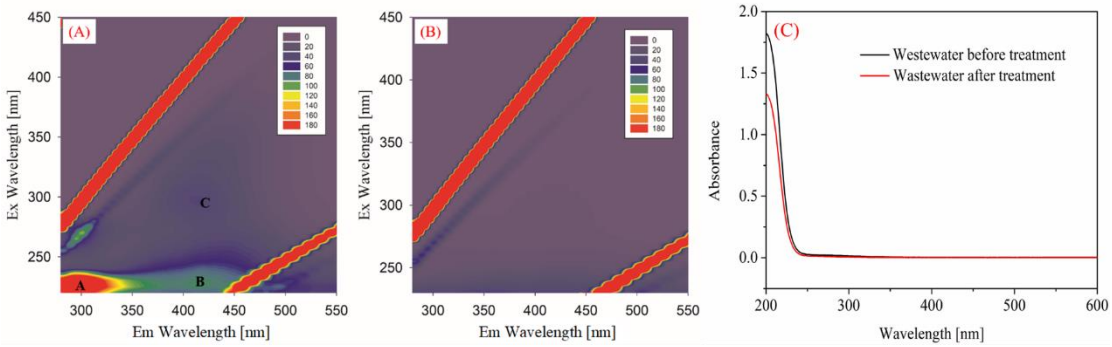

26 **Figure 5**

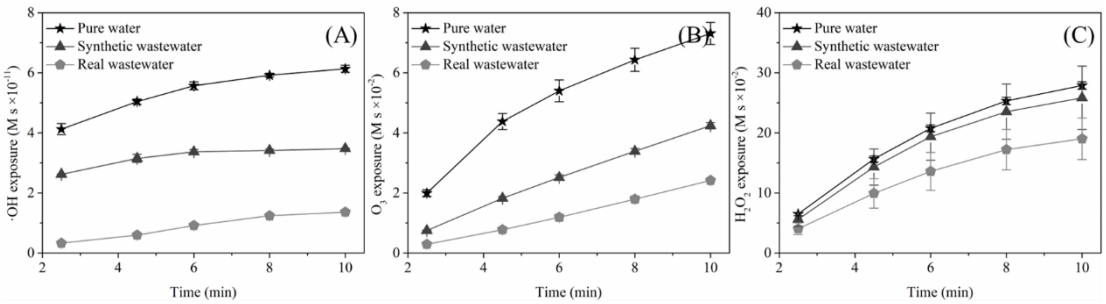

27

28 **Figure 6**

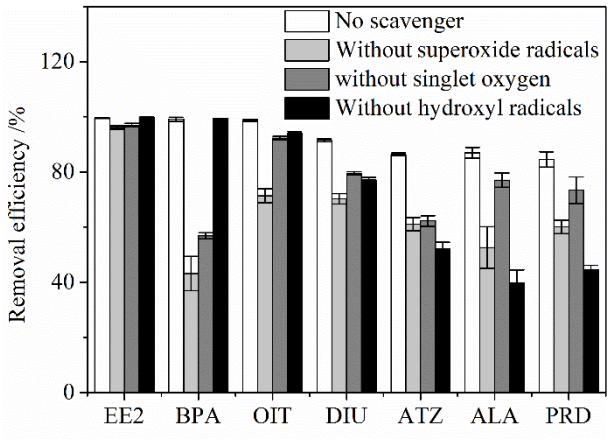

29

30 **Figure 7**

31 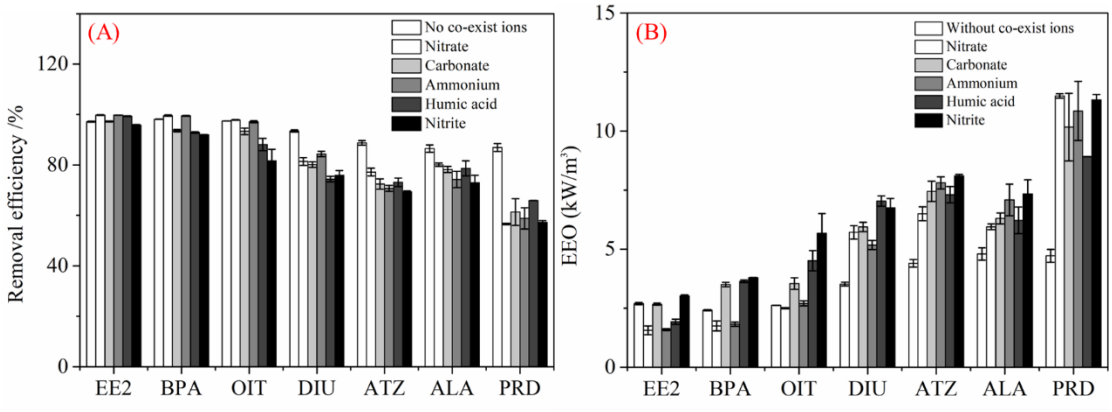

Reference

Vanraes, P., Ghodbane, H., Davister, D., Wardenier, N., Nikiforov, A., Verheust, Y.P., Van Hulle, S.W.H., Hamdaoui, O., Vandamme, J., Van Durme, J., Surmont, P., Lynen, F. and Leys, C. (2017) Removal of several pesticides in a falling water film DBD reactor with activated carbon textile: Energy efficiency. Water Res 116, 1-12.

Vanraes, P., Willems, G., Nikiforov, A., Surmont, P., Lynen, F., Vandamme, J., Van Durme, J., Verheust, Y.P., Van Hulle, S.W., Dumoulin, A. and Leys, C. (2015) Removal of atrazine in water by combination of activated carbon and dielectric barrier discharge. J Hazard Mater 299, 647-655.

Wardenier, N., Gorbanev, Y., Van Moer, I., Nikiforov, A., Van Hulle, S.W.H., Surmont, P., Lynen, F., Leys, C., Bogaerts, A. and Vanraes, P. (2019a) Removal of alachlor in water by non-thermal plasma: Reactive species and pathways in batch and continuous process. Water Res 161, 549-559.

Wardenier, N., Liu, Z., Nikiforov, A., Van Hulle, S.W.H. and Leys, C. (2019b) Micropollutant elimination by O3, UV and plasma-based AOPs: An evaluation of treatment and energy costs. Chemosphere 234, 715-724.

Wardenier, N., Vanraes, P., Nikiforov, A., Van Hulle, S.W.H. and Leys, C. (2019c) Removal of micropollutants from water in a continuous-flow electrical discharge reactor. J Hazard Mater 362, 238-245.

Table Captions

Table 1 Physical-chemical characteristics of the secondary effluent used in this work.

Table 2. Coded and actual levels of the independent variables for the design of the BBD experiment.

Table 3. The removal efficiency and energy consumption of μPs treated by nonthermal plasma-based AOPs in literature and this study.

Table 1

Parameters	pH	COD mg/L	NO_2^- mg N/L	NO_3^- mg N/L	NH_4^+ mg N/L
Values	6.9±0.2	39.0±4.5	0.02±0.01	25.4±0.8	0.57±0.01

Table 2

Independent variables	Symbol	Coded level		
		-1	0	-1
Gas flow (SLM*)	A	0.4	0.6	0.8
Liquid flow ($mL \cdot min^{-1}$)	B	60	80	100
Discharge power (W)	C	25	35	45

Note: * SLM: standard liter per minute.

Table 3

Micropollutants	Water matrix	Initial concentration µg/L	Removal efficiency /%	EE/O kW/m³	Ref
Diclofenac, Verapamil	Synthetic wastewater	1000	99	3.8	(Nippatlapalli et al. 2022)
Atrazine, Alachlor, Diuron, Dichlorvos, Pentachlorophenol, Carbamazepine, Bisphenol A, 1,7-α-ethinylestradiol	Synthetic wastewater	200	>92	2.4-4.2	(Wardenier et al. 2019)
Atrazine	Synthetic wastewater	20000	83	7.1	(Shen et al. 2022)
Alachlor, Diuron, isoproturon	Synthetic wastewater	100	65-95	4.6-17	(Vanraes et al. 2017)
meprobamate, Dilantin, Primidone, Carbamazepine, Atenolol, Trimethoprim, Atrazine	Secondary effluent	2-0.04	70-95	2.2-6.4	(Gerrity et al. 2010)
Diclofenac, Carbamazepine, Ciprofloxacin, Carbofuran, 2-4-D	Lake and river water	1000	>91	20-86	(Singh et al. 2019)
Atrazine, Alachlor, Diuron, primidone, bisphenol A, 1,7-α-ethinylestradiol, 2-n-octyl-4-isothiazolin-3-one	Synthetic wastewater	200	>85	2.3-4.8	This study
	Secondary effluent	200	>85	2.4-5.3	

Reference

Gerrity, D., Stanford, B.D., Trenholm, R.A. and Snyder, S.A. (2010) An evaluation of a pilot-scale nonthermal plasma advanced oxidation process for trace organic compound degradation. Water Res 44(2), 493-504.

Nippatlapalli, N., Ramakrishnan, K. and Philip, L. (2022) Enhanced degradation of complex organic compounds in wastewater using different novel continuous flow non – Thermal pulsed corona plasma discharge reactors. Environmental Research 203, 111807.

Shen, T., Wang, X., Xu, P., Yang, C., Li, J., Wang, P. and Zhang, G. (2022) Effect of dielectric barrier discharge plasma on persulfate activation for rapid degradation of atrazine: Optimization, mechanism and energy consumption. Environmental Research 212, 113287.

Singh, R.K., Philip, L. and Ramanujam, S. (2019) Continuous flow pulse corona discharge reactor for the tertiary treatment of drinking water: Insights on disinfection and emerging contaminants removal. Chemical Engineering Journal 355, 269-278.

Vanraes, P., Ghodbane, H., Davister, D., Wardenier, N., Nikiforov, A., Verheust, Y.P., Van Hulle, S.W.H., Hamdaoui, O., Vandamme, J., Van Durme, J., Surmont, P., Lynen, F. and Leys, C. (2017) Removal of several pesticides in a falling water film DBD reactor with activated carbon textile: Energy efficiency. Water Res 116, 1-12.

Wardenier, N., Vanraes, P., Nikiforov, A., Van Hulle, S.W.H. and Leys, C. (2019) Removal of micropollutants from water in a continuous-flow electrical discharge reactor. J Hazard Mater 362, 238-245.

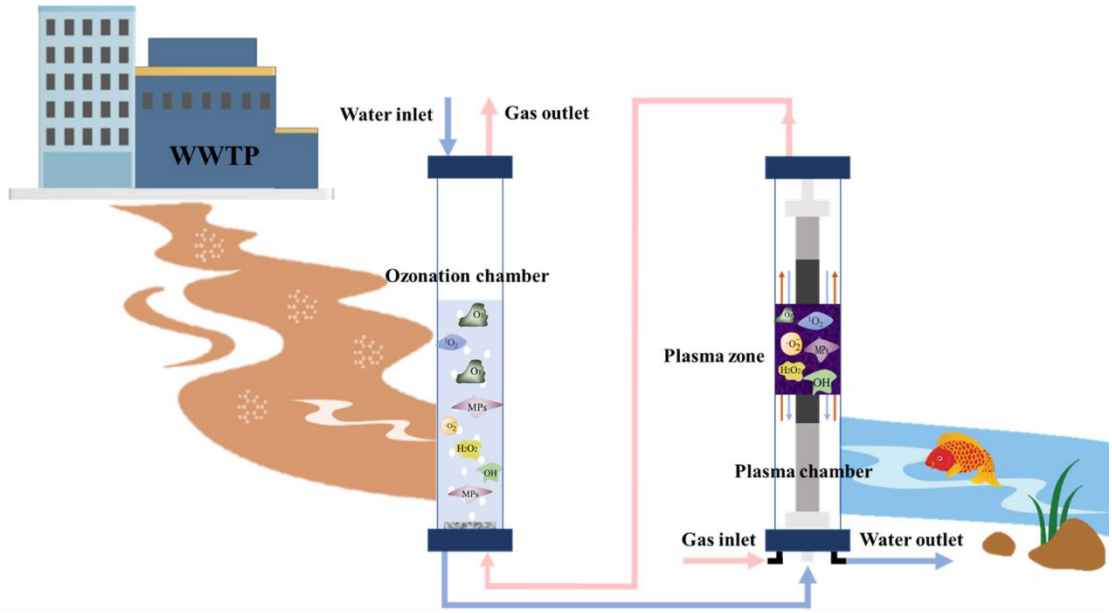
WWTP
Water inlet
Gas outlet
Ozonation chamber
Plasma zone
Plasma chamber
Gas inlet
Water outlet